

## Re-entry Guidance for Path-Constraint Tracking

Mooij, E.

**DOI**

[10.2514/6.2017-1265](https://doi.org/10.2514/6.2017-1265)

**Publication date**

2017

**Document Version**

Accepted author manuscript

**Published in**

AIAA Guidance, Navigation, and Control Conference, 2017

**Citation (APA)**

Mooij, E. (2017). Re-entry Guidance for Path-Constraint Tracking. In *AIAA Guidance, Navigation, and Control Conference, 2017* Article AIAA 2017-1265 American Institute of Aeronautics and Astronautics Inc. (AIAA). <https://doi.org/10.2514/6.2017-1265>

**Important note**

To cite this publication, please use the final published version (if applicable). Please check the document version above.

**Copyright**

Other than for strictly personal use, it is not permitted to download, forward or distribute the text or part of it, without the consent of the author(s) and/or copyright holder(s), unless the work is under an open content license such as Creative Commons.

**Takedown policy**

Please contact us and provide details if you believe this document breaches copyrights. We will remove access to the work immediately and investigate your claim.

# Re-entry Guidance for Path-Constraint Tracking

E. Mooij\*

*Delft University of Technology, Faculty of Aerospace Engineering,  
Kluyverweg 1, 2629 HS Delft, The Netherlands*

To limit the mass of the vehicle's thermal protection system, an optimal trajectory that minimises the total integrated heat load should be flown. In essence this boils down to tracking the maximum heat-flux constraint for as long as possible, until the maximum mechanical loads are encountered. Flying as close to this load as possible contributes to minimising the heat load as well. A combination of a semi-analytical guidance that produces nominal bank-angle commands and a tracking system based on a (linear) output-feedback controller is considered for tracking the path constraints. Both guidance components are reviewed and improved with respect to an earlier design. (Almost) discrete jumps in commanded bank angle are avoided by implementation of an analytical smooth step function. Transition from heat-flux tracking to controlling the maximum allowable  $g$ -load is achieved by a smooth interpolation between the respective tracking constants that are both a function of the product of atmospheric density and a polynomial term of flight velocity. The flight system under consideration is a hypersonic test vehicle of which the stagnation heat-flux should not exceed  $1,700 \text{ kW/m}^2$ , whereas the mechanical load should stay below  $5g$ . The results show that for a nominal mission the performance of both guidance components has been improved. Moreover, a Monte-Carlo analysis indicates that the tracking error for heat flux can be relatively small, and also the total integrated heat load can stay within limits. The  $g$ -load is never exceeding its constraint value.

## Nomenclature

<b>A</b>	system matrix
$a_\gamma$	normal acceleration other than from vertical lift, $\text{m/s}^2$
$a$	speed of sound, $\text{m/s}$
<b>B</b>	control matrix
<b>C</b>	output matrix
$c_1$	heat-flux constant
$c_2$	heat-flux exponent
$C_D$	drag coefficient
$C_L$	lift coefficient
$c_n$	value of $\rho V^n = \text{constant}$
$c_\gamma$	gain constant, $\text{s/rad}$
$D$	drag, $\text{N}$
$e_\gamma$	flight-path angle error, $\text{rad}$
$f_{n_g}$	transition percentage for $g$ -load
$g$	gravitational acceleration, $\text{m/s}^2$
$H_s$	atmospheric scale height, $\text{m}$
$h$	altitude, $\text{m}$
$h^*$	pseudo altitude, $\text{m}$
<b>K</b>	gain matrix
$K$	ballistic parameter, $\text{N/m}^2$
$K_\gamma$	flight-path angle gain, various (subscripts $p$ , $i$ , and $d$ for the PID compensator)
$K_n$	bank-angle gain, various (subscripts $p$ and $d$ for the PD compensator)

---

\*Assistant Professor, section Astrodynamics and Space Missions, e.mooij@tudelft.nl, Associate Fellow AIAA.

$L$	lift, N
$M$	Mach number
$m$	mass, kg
$n$	exponent in nominal-guidance law ( $n_1 = 6$ for heat flux, and $n_2 = 2$ for $g$ -load)
$n_g$	$g$ -load
$\mathbf{Q}$	state-deviation weighing matrix
$Q$	integrated heat load, J/m <sup>2</sup>
$q_c$	convective heat flux in stagnation point, W/m <sup>2</sup>
$\mathbf{R}$	control-effort weighing matrix
$R$	radial distance, m
$R_N$	nose radius, m
$t$	activation (index 1) and de-activation (index 2) time of heat-flux tracking, s
$t_f$	flight time, s
$\mathbf{u}$	control vector
$V$	velocity, m/s
$V_c$	local circular velocity, m/s
$\mathbf{x}$	state vector
$\mathbf{y}$	output vector
$\alpha$	angle of attack, rad
$\beta$	angle of sideslip, rad
$\gamma$	flight-path angle, rad
$\Delta..$	perturbed value
$\delta$	latitude, rad
$\zeta$	damping coefficient
$\rho$	atmospheric density, kg/m <sup>3</sup>
$\Sigma$	performance index
$\sigma$	bank angle, rad
$\tau$	longitude, rad
$\chi$	heading, rad
$\omega$	eigenfrequency, rad/s
$\omega_{cb}$	rotational rate of the Earth, rad/s

## I. Introduction

Satellites and other space vehicles that travel through the thicker layers of the atmosphere with high velocities are subject to large aerodynamic forces, and reach high temperatures as a result of aerodynamic heating due to friction. In general, these objects disintegrate and burn up completely, except for very large and very heavy parts. To safely reach the Earth's surface, accurate control over the trajectory is therefore mandatory. Moreover, to limit the mass of the vehicle's Thermal Protection System (TPS), an optimal trajectory that minimises the total integrated heat load should be flown. Also, to increase the number of reachable landing sites the vehicle should have maximum crossrange and downrange capabilities.

Minimising the integrated heat load can be achieved by flying at the maximum allowable heat flux, as this will greatly reduce the flight time and hence the thermal load. Tracking this heat-flux constraint in a robust manner is therefore key to a successful mission. However, the resulting trajectory will also induce relatively large mechanical loads, which should be constrained as well to avoid that the vehicle is getting damaged or worse yet, breaking up. Still, flying at the highest possible mechanical load is beneficial to reducing the integrated thermal load.

A straight-forward and simple implementation could be a (linear) output-feedback controller that has a fast response, although its robustness could be doubtful due to insufficient damping. Designing such a tracking guidance is easy due to the well established design methodology using optimal-control theory, leading to a linear quadratic regulator using output weighing. A possible good alternative is a guidance-tracking system based on so-called simple adaptive control (SAC),<sup>1</sup> which has shown a variety of applications in the field of, for instance, autopilot design<sup>2</sup> and entry systems.<sup>3,4</sup> Such a system is known to have an excellent performance under the influence of rather large uncertainties, although its transient response could

be sluggish at times. A potential problem, however, may be the large number of design parameters that can be tuned, without the existence of a proper design methodology.<sup>5</sup>

Previous work focussed on setting up a rudimentary nominal guidance scheme for heat-flux tracking and analysed the implementation of the aforementioned tracking systems, as well as an integrated approach combining the two to check whether the strong points of the individual systems could be combined.<sup>5</sup> Outcome of that study was that for a nominal mission the performance of the two individual tracking systems is equal. A Monte-Carlo analysis indicated that the tracking error is smaller for the output-feedback controller, but due to its longer tracking time the total heat load is smaller for the adaptive system. Integrating the two systems yielded a significant reduction of the tracking error, albeit at the expense of a larger guidance effort.

The current paper will build on those results, and address some of the shortcomings and limitations not covered earlier. First, the nominal guidance system is revisited to include the mechanical load next to the heat load. Since the induced loads are sensitive to discrete changes in the guidance commands, particular attention is paid to a smooth transition between the two phases. Second, the output-feedback tracking system is extended to include the mechanical load and to avoid disruptions due to switching from one mode to the other. The adaptive tracking is currently not addressed, but is seen as the next step in the ongoing research.

The layout of this paper is as follows. Section II will introduce the vehicle model and the equations of motion. In Section III, the guidance system is described, consisting of two parts: the nominal guidance and the tracking system based on linear output feedback. For both parts, the effect of the modifications is discussed. Section IV presents the results of a more extensive analysis of the integrated system. Section V, finally, concludes this paper.

## II. Model Description

### A. Vehicle and Mission

The vehicle that we consider in the present study is a small, low-cost re-entry testbed for hypersonic experiments, designated *Hyperion-1*, and originally studied in the mid and late nineties.<sup>6,7</sup> Purpose of this vehicle was to execute a wide range of experiments in hypersonic flight, otherwise not possible in ground-based facilities. Examples of such experiments are the testing of thermal-protection materials and coatings in a real-gas environment, aerodynamic measurements, such as boundary-layer transition and shockwave boundary-layer transition, and testing of new guidance, navigation and control (GNC) systems during re-entry.

The re-entry module has a triangular shape with rounded corners and has three flaps mounted on the base for aerodynamic control during atmospheric flight (Fig. 1). This configuration is particularly suitable for in-flight corrections of a possible misprediction of the centre of pressure (c.o.p.) by deflecting all three flaps to move the c.o.p. towards the correct location. Another important function of the flaps is the deceleration of the module during subsonic flight prior to parachute deployment. In the current study, however, we consider the vehicle configuration without flaps; control could be achieved by reaction-control thrusters or moving masses. The total vehicle mass is defined to be 450 kg. The aerodynamic properties of the base vehicle are based on the assumption of modified Newtonian flow, by taking only pressure forces into account and neglecting skin friction.

A typical reference scenario for an entry (test) vehicle could be one that maximises its flight range while at the same time minimising the integrated heat load. Such a flight can be achieved by flying along a maximum heat-flux constraint as long as possible, since this will minimise the total flight time. This maximum heat flux should, of course, be within the capabilities of the vehicle's thermal protection system; to lower the peak heat flux, the flight is initiated at maximum angle of attack. Once the peak heat-flux has passed, the angle of attack may be lowered to a value that will maximise the lift-to-drag ratio,  $L/D$ , a condition that maximises the flight range.

An example of such a reference mission is shown in Fig. 2. Besides the heat-flux constraint, also a maximum allowable mechanical load should be observed, as violating that constraint may lead to the destruction of the vehicle. From the plots, it is clear that *Hyperion-1* flies along the two active path constraints heat flux and  $g$ -load, although the flight along the  $g$ -load constraint is only brief. The small deviations from the constraints are easily attributed to the simplifications that were made while setting up the trajectory design (non-rotating Earth, exponential density profile, *etc.*). The time histories of the two constraints confirm the correctness of the trajectory design: the constraints are tracked well enough given the assumptions.

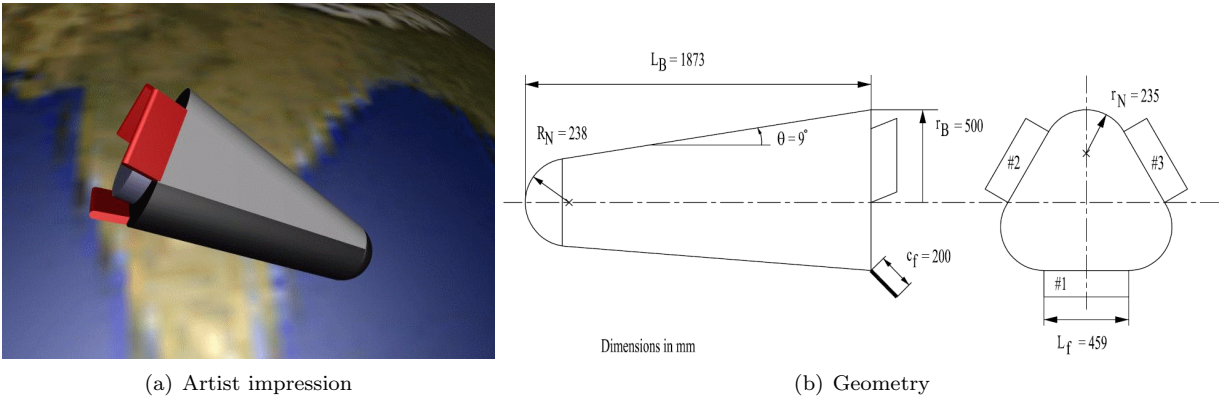


Figure 1. *Hyperion-1* re-entry vehicle.

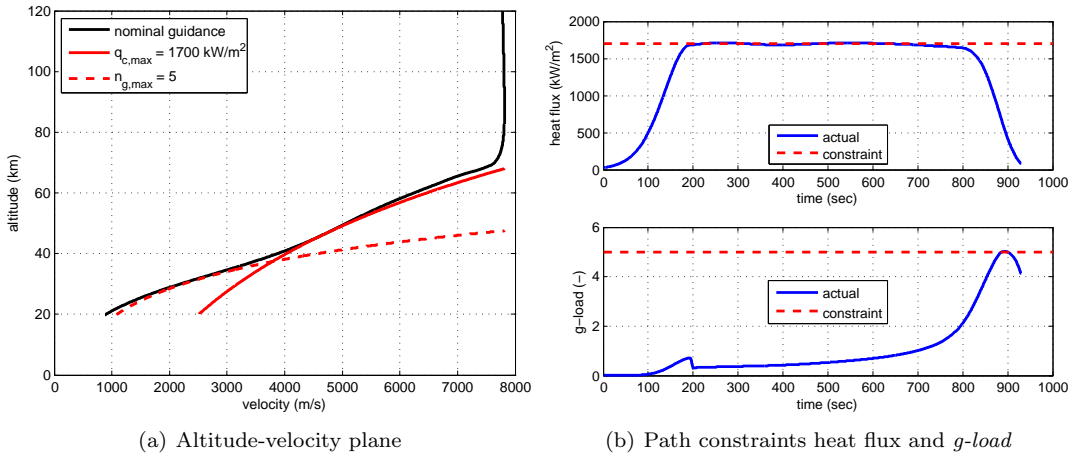


Figure 2. *Hyperion-1* reference trajectory.

## B. Flight Dynamics

The motion of re-entry vehicles is mainly driven by the combination of aerodynamic and gravitational forces and moments. Depending on the inherent non-linearities in the vehicle's aerodynamic characteristics, the extent of the flight regime under consideration, and asymmetry in the mass distribution of the vehicle, this motion can only be accurately described by a set of coupled first-order non-linear differential equations.

To describe the flight dynamics we use the position and velocity definition in spherical coordinates, see Fig. 3(a). This choice is primarily motivated by the fact to use the same model for the guidance-system development as well as simulating the flight dynamics. The position is defined by the distance  $R = R_e + h$ , longitude  $\tau$  and latitude  $\delta$ , whereas the velocity is expressed by its modulus, the groundspeed  $V_g$ , and two direction angles, *i.e.*, flight-path angle  $\gamma_g$  and heading  $\chi_g$  (note that since we do not consider wind, the subscript 'g' to differentiate between air- and groundspeed will be dropped). The attitude of the vehicle, or, in mathematical terms, the orientation of the body-fixed reference frame with respect to the trajectory reference frame, is expressed by the so-called aerodynamic angles, *i.e.*, the angle of attack  $\alpha$ , the angle of sideslip  $\beta$  and the bank angle  $\sigma$ , see also Fig. 3(b).

The dynamic equations of translational motion for a rotating, spherical Earth are given by<sup>8</sup>

$$\dot{V} = -\frac{D}{m} - g \sin \gamma + \omega_{cb}^2 R \cos \delta (\sin \gamma \cos \delta - \cos \gamma \sin \delta \cos \chi) \quad (1)$$

$$\dot{\gamma} = \frac{L \cos \sigma}{mV} - \frac{g}{V} \cos \gamma + 2\omega_{cb} \cos \delta \sin \chi + \frac{V}{R} \cos \gamma + \omega_{cb}^2 \frac{R}{V} \cos \delta (\cos \delta \cos \gamma + \sin \gamma \sin \delta \cos \chi) \quad (2)$$

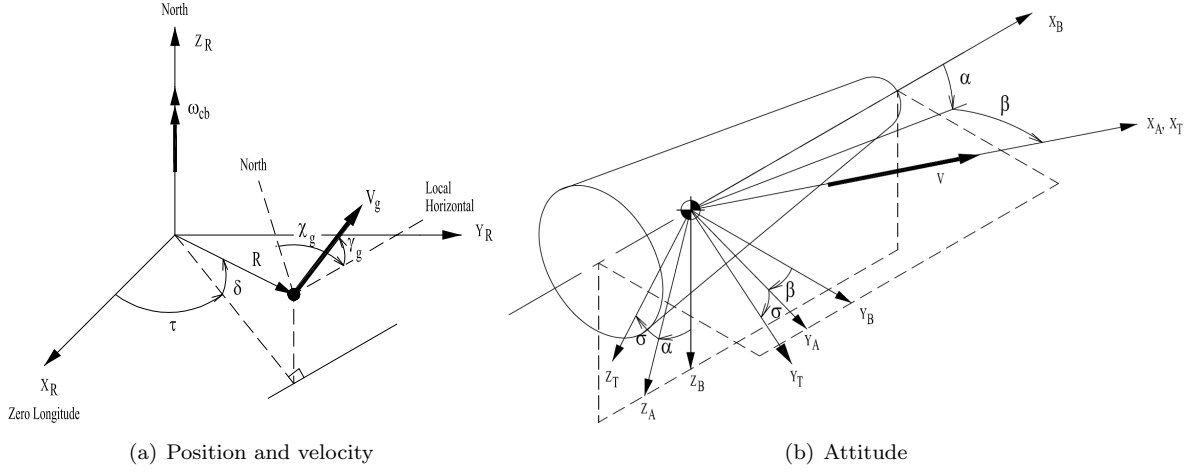


Figure 3. Definition of state variables.

$$\dot{\chi} = \frac{L \sin \sigma}{mV \cos \gamma} + 2\omega_{cb}(\sin \delta - \cos \delta \tan \gamma \cos \chi) + \frac{V}{R} \cos \gamma \tan \delta \sin \chi + \omega_{cb}^2 \frac{R}{V \cos \gamma} \cos \delta \sin \delta \sin \chi \quad (3)$$

whereas the kinematic position equations are given by

$$\dot{R} = \dot{h} = V \sin \gamma \quad (4)$$

$$\dot{\tau} = \frac{V \sin \chi \cos \gamma}{R \cos \delta} \quad (5)$$

$$\dot{\delta} = \frac{V \cos \chi \cos \gamma}{R} \quad (6)$$

In the above equations  $D$  and  $L$  are the aerodynamic drag and lift in N,  $g$  is the gravitational acceleration in  $\text{m/s}^2$ , and  $\omega_{cb}$  is the rotational rate of the Earth in  $\text{rad/s}$ .

### III. Guidance System

The guidance system for *Hyperion* consists of a nominal guidance that produces the reference commands (and thus a reference trajectory that meets with the path constraints), and a tracking system, which guarantees that the reference profile is followed as closely as possible. The basis for this guidance system has been discussed in previous work,<sup>5</sup> albeit for heat-flux tracking only. In the current paper, the guidance system is extended with the capabilities of tracking a mechanical-load limit. The remainder of this section addresses both elements of the guidance system, *i.e.*, Sec. III.A reviews the nominal guidance and introduces some improvements, whereas the tracking guidance is discussed in Sec. III.B for a linear output feedback system.

#### A. Nominal Guidance

For determining the reference trajectory, we will set up a trajectory that combines the aspects of minimum heat load and maximum range. Of course, since these two objectives are partly conflicting, the resulting trajectory will not be optimal in both objectives, but will give a good compromise that can be used as a starting point for further mission analysis. The initial position and velocity of the vehicle at the entry interface will be typical low Earth orbit (LEO) re-entry conditions,<sup>6</sup> *i.e.*,  $h = 119.81$  km,  $\tau = -119.5^\circ$ ,  $\delta = 7.56^\circ$ ,  $V = 7,782.5$  m/s,  $\gamma = -2.87^\circ$  and  $\chi = 90.18^\circ$ .

In this study no landing site will be specified, as we want to optimise the cross- and downrange of the vehicle by modulating angle of attack and bank angle. During re-entry the vehicle will encounter several kinds of loads. These loads are usually not allowed to exceed certain values, *i.e.*, the *flight-path constraints*.

In determining the analytical benchmark, we will consider two flight-path constraints, *i.e.*, the heat flux and the *g-load*. For the heat flux  $q_c$  the (cold-wall) Chapman model is used as a first approximation:

$$q_c = \frac{c_1}{\sqrt{R_N}} \sqrt{\frac{\rho}{\rho_0}} \left( \frac{V}{V_c} \right)^{c_2} = c^* \sqrt{\rho} V^{c_2} \quad (7)$$

with  $c_1 = 1.06584 \cdot 10^8 \text{ W/m}^{3/2}$ ,  $R_N = \text{nose radius} = 0.238 \text{ m}$ ,  $\rho = \text{atmospheric density (kg/m}^3\text{)}$ ,  $\rho_0 = \text{density at sea level} = 1.225 \text{ kg/m}^3$ ,  $V_c = \text{circular velocity at re-entry} = 7,905 \text{ m/s}$ , and  $c_2 = 3$ .

The *g-load*  $n_g$  is defined to be the normalised acceleration due to the aerodynamic forces, *i.e.*,

$$n_g = \frac{\sqrt{D^2 + L^2}}{mg_0} = \frac{\sqrt{C_D^2 + C_L^2}}{mg_0} \rho V^2 S_{ref} \quad (8)$$

where  $C_D$  and  $C_L$  are the drag and lift coefficient,  $S_{ref}$  is the aerodynamic reference area,  $m$  is the vehicle mass and  $g_0 = 9.81 \text{ m/s}^2$  is the standard gravitational acceleration at the Earth's surface.

In the current study, the maximum heat flux is set to  $1,700 \text{ kW/m}^2$ . This heat flux corresponds with a (maximum) wall temperature of about  $2,400 \text{ K}$  according to the Stefan-Boltzman Law (with an emissivity of  $0.85$  and neglecting the local atmospheric temperature). However, this flux represents a stagnation-point flux only, and further away from this point the flux will reduce to lower values that can be withstood with a good TPS design. The maximum *g-load* is set to  $n_g = 5$ .

The above constraints can be simplified by assuming a constant circular velocity ( $V_c = 7,905 \text{ m/s}$ , the value at the entry interface), as well as constant (hypersonic)  $C_D$  and  $C_L$ . This is a good approximation because down to  $M \approx 5$  the aerodynamic characteristics are almost constant (the Mach independence principle). This means that along the *g-load* constraint, the dynamic pressure is constant. Summarised, the constraints can thus be written as:

$$q_c = c_{q_c} \sqrt{\rho} V^3 \quad \text{and} \quad n_g = c_g \rho V^2 \quad (9)$$

The nominal guidance is set up as follows. At entry, the angle of attack will be at its maximum value ( $\alpha = 45^\circ$ ), to get the maximum lift. This will minimise the maximum occurring heat flux. When the largest heat flux has been reached, a flight at maximum  $L/D$  will be started to maximise the cross- and downrange. The bank angle is modulated, first to fly along the maximum heat-flux constraint, and later on to stay below the *g-load* constraint. The bank-angle control to follow the path constraints has been derived in an analytical form, based on simplified equations of motion. The solution is based on the fact that for both path constraints the term  $\rho V^n$  is constant. For the heat flux  $n = 6$  and for the *g-load*  $n = 2$ , see Eq. (9). Further, we assume that

1. the Earth is non-rotating
2. there is a central gravity field
3. the atmospheric density  $\rho$  follows an exponential profile<sup>a</sup>, *i.e.*,  $\rho = \rho_0 e^{-h/H_s}$  ( $\rho_0 = 1.225 \text{ kg/m}^3$  is the atmospheric density at sea level, and  $H_s = 7,050 \text{ m}$  is the scale height).

Based on a simplified differential equation for the acceleration:

$$\dot{V} = -\frac{D}{m} - g \sin \gamma = -\frac{\rho V^2}{2K} - g \sin \gamma = -\frac{c_n}{2KV^{n-2}} - g \sin \gamma \quad (10)$$

where  $K = \frac{m}{C_D S_{ref}}$  = ballistic coefficient ( $\text{kg/m}^2$ ),  $g$  = local gravity acceleration ( $\text{m/s}^2$ ),  $c_n = \rho V^n = \text{constant}$ . From the condition  $\rho V^n = \text{constant}$  we derive:

$$\frac{d(\rho V^n)}{dt} = \frac{d\rho}{dh} h V^n + n \rho V^{n-1} \dot{V} = 0 \quad (11)$$

For an exponential atmosphere,  $\frac{d\rho}{dh} = -\frac{\rho}{H_s}$ , and with Eqs. (4) and (10) substituted, this results in:

$$-\frac{\rho}{H_s} V^{n+1} \sin \gamma - n \rho V^{n-1} \left( \frac{c_n}{2KV^{n-2}} - g \sin \gamma \right) = 0 \quad (12)$$

---

<sup>a</sup>An exponential atmosphere is in essence an isothermal atmosphere, implying the temperature (and thus the speed of sound) is constant

Re-arranging terms yields for the "commanded" flight-path angle that fulfills the tracking criterion:

$$\sin \gamma_c = -c_n \frac{n}{V^{n-2}} \frac{H_s}{2K} \frac{1}{V^2 - ngH_s} \quad (13)$$

To link this commanded flight path with the external forces, most notably the vertical lift force that will provide us with a commanded bank angle,  $\sigma_{0,c}$ , we take the derivative of Eq. (13) with respect to velocity,

$$\left. \frac{d\gamma}{dV} \right|_c = \frac{c_n}{\cos \gamma_c} \left\{ \frac{2n^2KH_s(V^{n-1} + gH_s(n-2)V^{n-3})}{[2KV^{n-2}(V^2 + gnH_s)]^2} \right\} \quad (14)$$

Because the time derivative of  $\gamma$  can be written as  $\dot{\gamma} = \frac{d\gamma}{dV} \dot{V}$ , the value of  $\sigma_{0,c}$  can be found from the differential equations for  $\gamma$ , Eq. (2), and  $V$ , Eq. (1). In this case we do take the accelerations due to the rotation of the Earth into account to minimise the deviation from the actual flight path:

$$V \left. \frac{d\gamma}{dt} \right|_c = \frac{L \cos \sigma_{0,c}}{m} + \sum (a_\gamma)_i \quad (15)$$

with  $\sum_i (a_\gamma)_i$  being the sum of all acceleration terms other than the vertical-lift acceleration:

$$\sum_i (a_\gamma)_i = -g \cos \gamma_c + 2\omega_{cb}V \cos \delta \sin \chi + \frac{V^2}{R} \cos \gamma_c + \omega_{cb}^2 R \cos \delta (\cos \delta \cos \gamma_c + \sin \gamma_c \sin \delta \cos \chi) \quad (16)$$

Isolating the bank angle yields:

$$\cos \sigma_{0,c} = \frac{m}{L} \left[ \left. \frac{d\gamma}{dt} \right|_c - \sum_i (a_\gamma)_i \right] = \frac{m}{L} \left[ \left. \frac{d\gamma}{dV} \right|_c \dot{V} - \sum_i (a_\gamma)_i \right] \quad (17)$$

The above guidance law assumes not only a commanded flight-path angle rate, but also a reference value for the flight-path angle itself,  $\gamma_c$ . This  $\gamma_c$  may be different from the actual flight-path angle, due to uncertainties in environment or vehicle characteristics, and to compensate for this difference a small correction term,  $\Delta\dot{\gamma}_c$ , may be added to  $\dot{\gamma}_c$ , given by Eq. (15). Let the error in flight-path angle be defined as  $e_\gamma = \gamma_c - \gamma$ . We can then define a PID compensator in the form of

$$\Delta\dot{\gamma}_c = K_{\gamma p} e_\gamma + K_{\gamma i} \int_0^t e_\gamma dt + K_{\gamma d} \frac{de_\gamma}{dt} \quad (18)$$

To determine the feedback gains,  $K_{\gamma p}$ ,  $K_{\gamma i}$  and  $K_{\gamma d}$ , it suffices to look at the open-loop transfer function of the gamma-error to gamma-rate block. After Laplace transformation, Eq. (18) becomes:

$$\dot{\gamma}_c(s) = s\gamma_c(s) = \left( K_{\gamma p} + \frac{K_{\gamma i}}{s} + sK_{\gamma d} \right) (\gamma_c(s) - \gamma(s)) \quad (19)$$

so:

$$H_{\gamma, \gamma_c}(s) = \frac{\gamma_c(s)}{\gamma(s)} = \frac{s^2 K_{\gamma d} + sK_{\gamma p} + K_{\gamma i}}{s^2(K_{\gamma d} - 1) + sK_{\gamma p} + K_{\gamma i}} = \frac{s^2 \frac{K_{\gamma d}}{K_{\gamma d} - 1} + s \frac{K_{\gamma p}}{K_{\gamma d} - 1} + \frac{K_{\gamma i}}{K_{\gamma d} - 1}}{s^2 + s \frac{K_{\gamma p}}{K_{\gamma d} - 1} + \frac{K_{\gamma i}}{K_{\gamma d} - 1}} \quad (20)$$

Equating the denominator with a standard second-order characteristic equation, *i.e.*,

$$s^2 + 2\zeta_\gamma \omega_\gamma s + \omega_\gamma^2 = s^2 + s \frac{K_{\gamma p}}{K_{\gamma d} - 1} + \frac{K_{\gamma i}}{K_{\gamma d} - 1} \quad (21)$$

gives us two equations with three unknowns. To solve for  $K_{\gamma p}$ ,  $K_{\gamma i}$  and  $K_{\gamma d}$ , the damping and frequency of the open-loop harmonic response,  $\zeta_\gamma$  and  $\omega_\gamma$ , as well as one of the three gains has to be specified. Using a PI regulator, it was found that for  $\zeta_\gamma = 0.7$  and  $\omega_\gamma = 1.35$  rad/s, the system was indeed functioning properly. In the current application, though, a PID regulator is used with  $K_{\gamma p} = 6$  s<sup>-1</sup>,  $K_{\gamma i} = 2$  s<sup>-2</sup> and  $K_{\gamma d} = 0.2$ .

At the transition from constant heat flux ( $\rho V^6 = \text{const.}$ ) to constant *g-load* ( $\rho V^2 = \text{const.}$ ), a smooth transition of the bank-angle signal has to be modeled to avoid spikes in the guidance commands. In the original implementation, a weighted average between the two phases was implemented that works reasonably

well. However, from preliminary results it became evident that the  $g$ -load is rapidly increasing towards the end of the constant-heat-flux phase, see again Fig. 2, even though the transition is initiated when the actual acceleration is only 20% of  $n_{g,max}$  ( $f_{n_g} = 0.2$ ). A better alternative to the original weighted average may be to adapt the exponent  $n$  and to adjust the tracking constant  $\rho V^n$ . So, during the transition from  $n_1 = 6$  to  $n_2 = 2$  an intermediate value for  $n$  is calculated according to a so-called *smooth* step function<sup>b</sup>. With an argument  $n_x$ , normalised between 0 and 1, the smooth transition of  $n_g$  is given by

$$n_x = \frac{n_g - f_{n_g} n_{g,max}}{n_{g,max} - f_{n_g} n_{g,max}} \quad (22)$$

$$n_{trans} = n_1 - (n_1 - n_2) n_x^3 (6n_x^2 - 15n_x + 10) \quad (23)$$

and the corresponding tracking constant

$$c_{n,trans} = \rho V^{n_{trans}} \quad (24)$$

These values for  $n_{trans}$  and  $c_{n,trans}$  replace the corresponding values in Eq. (14), but other than that the algorithm remains the same. It was observed that at the initiation of the transition, the tracking constant discretely jumps to a lower value, because due to the assumptions in the development of the nominal guidance the maximum heat flux is not perfectly tracked. To avoid a discrete change in  $\sigma_c$ , a possible solution is to also apply a smooth step function to this constant. However, when the nominal guidance is combined with a tracking algorithm this change in constant is minimal and poses no problem. It remains to be studied, though, where in the algorithm smooth step functions could be used to guarantee a robust performance in the presence of (discrete) uncertainties and perturbations.

The last addition to the nominal guidance system is to add some damping in case at any time – but mostly in the transition phase – the tracking constant,  $c_n$ , changes rapidly. A simple PD regulator on the (normalised) tracking constant suffices for now, *i.e.*,

$$\sigma_c = \sigma_{0,c} + K_{np} \frac{c_{n,act} - c_n}{c_n} + K_{nd} \frac{\dot{c}_{n,act}}{c_n} \quad (25)$$

where  $\sigma_{0,c}$  is given by Eq. (17). Reasonable values for  $K_{np}$  and  $K_{nd}$  are -1 and 2, respectively.

To compare the performance of the nominal guidance, in Fig. 4 a comparison between the old and the new implementation is shown. In the left plot the relative heat-flux difference with respect to the setpoint of 1,700 kW/m<sup>2</sup> is shown. The new implementation is smoother, although it moves away from the set point earlier than the baseline implementation. This is purely initiated by the transition phase: it can be seen in the middle plot that the  $g$ -load does not increase nearly as much with the new implementation. It is clear that in the old version, there is a rapid increase towards the set point of  $n_g = 5$  g. As a consequence, in case of perturbations it might be difficult to keep  $n_g$  below the set point. With a larger margin, this potential problem is alleviated albeit at the expense of a slightly larger heat load (longer flight time).

In the right plot, the commanded bank angle is shown. The lower actual  $g$ -load requires a smaller bank angle, of course. Previously, the bank angle increased to a value for a lift-down configuration, but now it "only" goes to a horizontal orientation, leaving enough margin for the tracking guidance. The small spikes in  $\sigma_c$  are due to discrete changes in  $c_n$  (at  $t \approx 720$  s) and the use of the PD compensator for  $\sigma_c$ , Eq. (25), most notably due to the derivative term. Decreasing  $K_{nd}$  reduces these spikes, but will increase the  $g$ -load again. For now we leave it as it is, because abrupt changes may also occur due to the tracking guidance and the corrective guidance commands may even remove these spikes. For an actual implementation one could consider, for instance, to filter  $\sigma_c$  with a low-pass filter, but this remains to be done as future work. On a final note: since no lateral-guidance logic has been implemented, the bank angle will not change sign. Reversals might be required once a proper mission has been defined.

## B. Output Feedback Tracking

The tracking guidance is based on output feedback, where the deviation from the nominal heat flux and/or maximum  $g$ -load is countered by a corrective angle-of-attack and bank-angle command that affect the magni-

<sup>b</sup>In computer graphics, a smooth step function is often used in procedural textures to avoid sharp transitions. Ken Perlin, in Ref. 9, suggests a fifth-order polynomial function, which has zero 1<sup>st</sup>- and 2<sup>nd</sup>-order derivatives at  $x = 0$  and  $x = 1$ :  $f(x) = 6x^5 - 15x^4 + 10x^3$ .

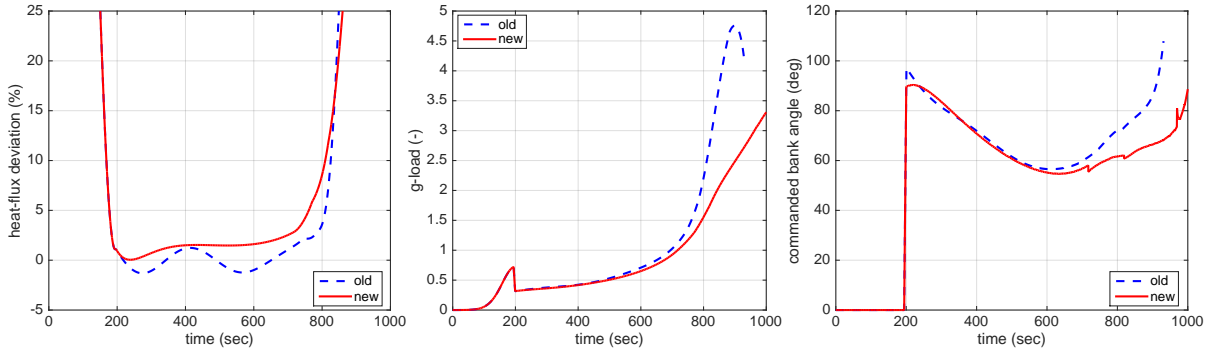


Figure 4. Effect of changes on nominal guidance system.

tude and orientation of the aerodynamic force components,  $D$  and  $L$ . The following guidance law represents this situation:

$$\Delta \mathbf{u} = -\mathbf{K}\Delta \mathbf{y} \quad (26)$$

where  $\Delta \mathbf{y}$  is the deviation from the nominal output, yielding a corrective guidance command  $\Delta \mathbf{u}$ . The gain matrix  $\mathbf{K}$  can be obtained by specifying the maximum output deviation  $\Delta \mathbf{y}_{max}$  and control effort  $\Delta \mathbf{u}_{max}$ , and solving the optimal cost criterion for a linearised system:

$$\Delta \dot{\mathbf{x}} = \mathbf{A}\Delta \mathbf{x} + \mathbf{B}\Delta \mathbf{u} \quad \Delta \mathbf{y} = \mathbf{C}\Delta \mathbf{x} \quad (27)$$

The resulting controller is known as a linear quadratic output regulator (LQY). It is noted that rather than using the states  $V$ ,  $\gamma$ , and  $h$  for vertical motion, the flight-path angle and altitude are combined into a so-called pseudo altitude,  $h^*$ . Reason for doing so is that  $h$  is not directly controllable, only through a change in  $\gamma$ , so merging the two will give a more unified approach. So:

$$h^* = h + K_\gamma \gamma \quad (28)$$

where  $K_\gamma$  is a velocity-dependent gain, *i.e.*,  $K_\gamma = c_\gamma V$  m/rad; a value of  $c_\gamma = 20$  s/rad is found to work well for this type of vehicle-mission combination.

The basis for the LQY development follows from taking the time derivative of Eq. (28) and combining this with Eqs. (2) and (6). Assuming a non-rotating Earth yields the following two equations for vertical motion:<sup>5</sup>

$$\dot{V} = -g \sin \gamma - \frac{D}{m} \quad (29)$$

$$\dot{h}^* = V \sin \gamma + c_\gamma \left[ \frac{V^2}{R} \cos \gamma - g \cos \gamma + \frac{L}{m} \cos \sigma \right] + c_\gamma \gamma \dot{V} \quad (30)$$

where we kept  $\dot{V}$  in Eq. (30) to facilitate the linearisation. The partials with respect to  $h^*$  are obtained from

$$\frac{\partial \dot{V}}{\partial h^*} = \frac{\partial \dot{V}}{\partial h} \frac{\partial h}{\partial h^*} + \frac{\partial \dot{V}}{\partial \gamma} \frac{\partial \gamma}{\partial h^*} \quad (31)$$

$$\frac{\partial \dot{h}^*}{\partial h^*} = \frac{\partial \dot{h}^*}{\partial h} \frac{\partial h}{\partial h^*} + \frac{\partial \dot{h}^*}{\partial \gamma} \frac{\partial \gamma}{\partial h^*} \quad (32)$$

with

$$\left. \frac{\partial h}{\partial h^*} \right|_0 = 1 \quad \text{and} \quad \left. \frac{\partial \gamma}{\partial h^*} \right|_0 = \frac{1}{c_\gamma V_0}$$

The partial derivative of  $\dot{V}$  with respect to  $V$  will also include a partial with respect to  $\gamma$ , because  $\gamma$  is no longer an independent state, but has a dependence on  $V$  through Eq. (28). This means

$$\gamma = \frac{h^* - h}{c_\gamma V} \Rightarrow \left. \frac{\partial \gamma}{\partial V} \right|_0 = -\frac{\gamma_0}{V_0}$$

and, for instance,

$$\left. \frac{\partial(\sin \gamma)}{\partial V} \right|_0 = -\frac{\gamma_0}{V_0} \cos \gamma_0$$

Finally, for the sake of linearisation we will again assume an exponential atmosphere:

$$\rho = \rho_0 e^{-\frac{h}{H_s}} \quad (33)$$

As a result of using this density model

$$\frac{d\rho}{dh^*} = \frac{d\rho}{dh} \frac{dh}{dh^*} = -\frac{\rho}{H_s} \quad (34)$$

because  $\frac{dh}{dh^*} = 1$ . However, again we need to include the velocity dependency in the definition of  $h^*$ , so:

$$\frac{d\rho}{dV} = \frac{d\rho}{dh^*} \frac{dh^*}{dV} = -\frac{\rho c_\gamma \gamma}{H_s} \quad (35)$$

The system and control matrices,  $\mathbf{A}$  and  $\mathbf{B}$ , have been derived earlier and, to save space, can be found elsewhere.<sup>5</sup> Besides formulating the equations of motion in state-space form to calculate the gain matrix  $\mathbf{K}$ , also the outputs  $q_c$ , Eq. (7), and  $n_g$ , Eq. (8), have to be linearised to obtain the output matrix,  $\mathbf{C}$ . Because the tracking guidance is only active when flying along the heat-flux constraint,  $q_{c,max}$ , or when an overshoot of the maximum  $g$ -load,  $n_{g,max}$  is expected, these values are of course the nominal values. So:

$$\mathbf{C} = \begin{bmatrix} \frac{\partial q_c}{\partial V} & \frac{\partial q_c}{\partial h^*} \\ \frac{\partial n_g}{\partial V} & \frac{\partial n_g}{\partial h^*} \end{bmatrix}_{\mathbf{x}=\mathbf{x}_0, \mathbf{u}=\mathbf{u}_0} \quad (36)$$

Consequently, linearising Eqs. (7) and (8) yields:

$$\mathbf{C} = \begin{bmatrix} q_{c,max} & n_{g,max} \end{bmatrix} \begin{bmatrix} \frac{3}{V_0} - \frac{c_\gamma \gamma_0}{2H_s} & \frac{3}{c_\gamma \gamma_0 V_0} - \frac{1}{2H_s} \\ \frac{2}{V_0} - \frac{c_\gamma \gamma_0}{H_s} & -\frac{1}{H_s} \end{bmatrix} \quad (37)$$

With the definition of two weighing matrices  $\mathbf{Q}$  and  $\mathbf{R}$  as

$$\mathbf{Q} = \text{diag} \left\{ \frac{1}{\Delta q_{c,max}^2} \quad \frac{1}{\Delta n_{g,max}^2} \right\} \quad (38)$$

$$\mathbf{R} = \text{diag} \left\{ \frac{1}{\Delta \alpha_{max}^2} \quad \frac{1}{\Delta \sigma_{max}^2} \right\} \quad (39)$$

we can solve the Riccati equation to obtain  $\mathbf{K}$ . In the current paper the input values used are  $\Delta q_{c,max} = 2,500 \text{ W/m}^2$ ,  $\Delta n_{g,max} = 0.2 \text{ g}$ ,  $\Delta \alpha_{max} = 5^\circ$  and  $\Delta \sigma_{max} = 20^\circ$ .

The "nominal mission" as discussed in the previous section will now be simulated with the LQY tracking active, for both versions of the nominal guidance. The results are shown in Fig. 5. With the original nominal guidance system and no changes to the tracking system defined above (and also used in Ref. 5), the  $g$ -load overshoots its maximum allowable value (compare also the plots shown in Fig. 5). With the adjustments in the nominal guidance, *i.e.*, the delay in increasing  $g$ -load, the tracking system does not introduce additional problems. However, the way the tracking is implemented does cause large jumps in  $\sigma_c$ . Towards the end of the heat-flux tracking  $q_c$  rapidly decreases, and tracking the growing error is no longer within the vehicle's capabilities. So, therefore the tracking is stopped at that moment, but the discrete jump to a zero error is, of course, not a proper solution.

A minor adjustment is to smoothly decrease the error to zero from the moment the tracking would normally stop, currently set at the condition when  $q_c$  has reduced to 90% of the set point and is reducing at a rate larger than  $\dot{q}_c = -2 \text{ kW/s}$ . The error at that moment,  $\Delta q_{c,f}$ , is fed through a smooth step function, similar to the one described by Eq. (23):

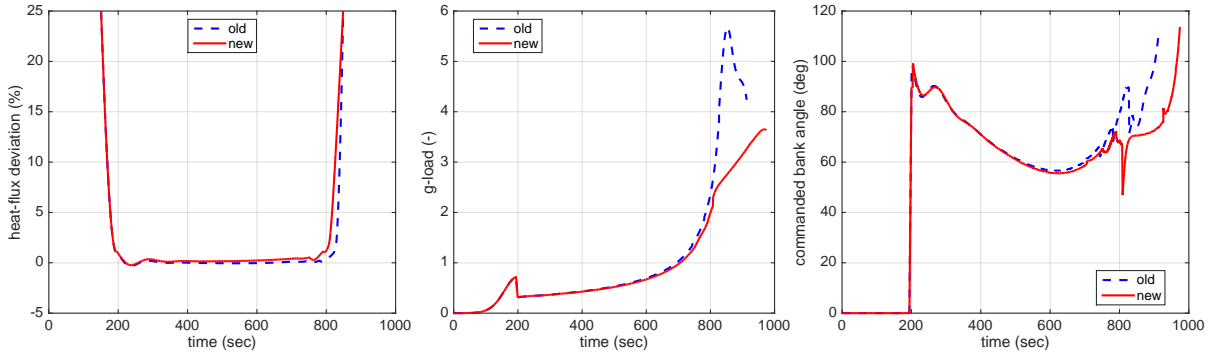


Figure 5. Nominal mission tracking for two versions of the nominal guidance system.

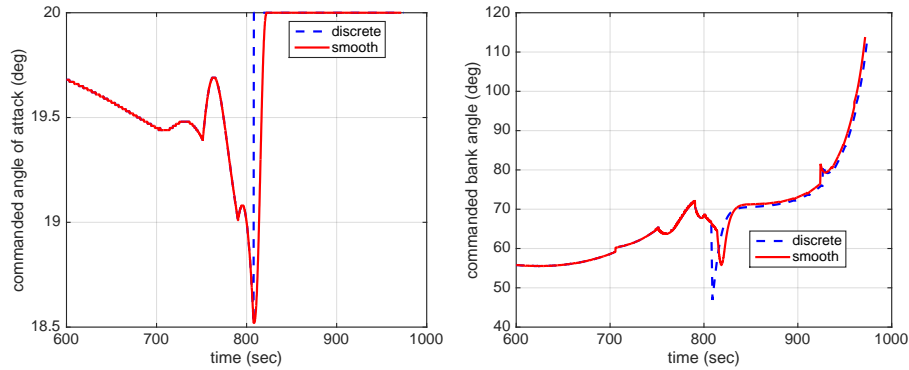


Figure 6. Output-feedback tracking with and without final-error smoothing.

$$\Delta q_c^* = \Delta q_{c,f} [1 - t_q^3 (6t_q^2 - 15t_q + 10)] \quad (40)$$

where  $t_q$  is the normalised decay time (ranging from 0 to 1, scaled with the total decay duration of  $\Delta t_q = 15$  s). Applying the smoothing, the guidance commands shown in Fig. 6 are obtained. The sharp peak in  $\sigma_c$  is gone, and inspecting the  $g$ -load does not show an increase in maximum value. The change in the  $\alpha_c$ -profile is less prominent, although the "discrete jump" is a bit more relaxed. It is noted that this smoothing function may easily be applied at more places in the algorithm to remove any discrete transitions in guidance commands. This particular improvement remains to be done as future work, though.

## IV. Sensitivity Analysis

In the previous section the performance improvements of the nominal guidance and the LQY tracking have been discussed. In the current section the results of a sensitivity analysis will be discussed, and compared with results obtained earlier.<sup>5</sup> The applied uncertainties are in the vehicle mass ( $\Delta m = \pm 20$  kg), the atmospheric density ( $\Delta \rho = \pm 15\%$ ), the speed of sound ( $\Delta a = \pm 10\%$ ), and the drag and lift coefficient ( $\Delta C_D, \Delta C_L = \pm 10\%$ ), each with a uniform distribution. Even though no navigation system has been implemented, the guidance system uses nominal values of  $C_D, C_L, \rho$  (and thus  $\bar{q}$ ), and  $a$  (and thus the Mach number,  $M$ ). The only exception is  $q_c$ , which is assumed to be coming from ideal measurements.

The performance of the tracking system is judged using several performance indices. The first one is the integrated heat load,  $Q$ , which should be as low as possible to minimise the mass of the thermal protection system. Because this is achieved by flying along the heat-flux constraint, the second performance index is the integrated heat-flux deviation from this constraint. Mathematically this index is defined as

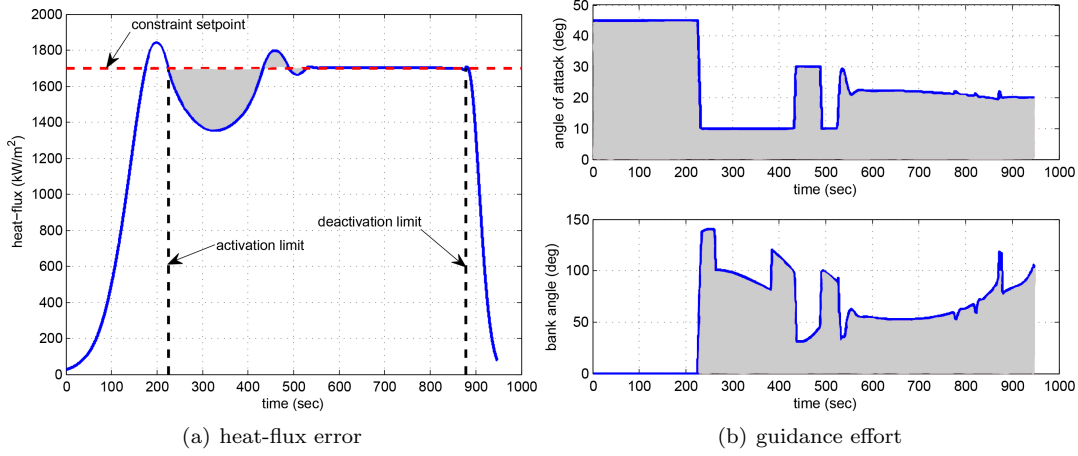


Figure 7. Integrated performance indices, represented by the shaded areas.

$$\sum_{q_{c,err}} = \int_{t_1}^{t_2} \sqrt{(q_c - q_{c,max})^2} dt \quad (41)$$

with  $t_1$  and  $t_2$  the activation and de-activation time of the heat-flux tracking. This index has been visualised in Fig. 7(a), where the shaded area corresponds with Eq. (41). For the  $g$ -load tracking it is sufficient to integrate only the overshoots, because having a  $g$ -load smaller than  $n_{g,max}$  should not be penalised. Thus, the third performance index is:

$$\sum_{n_{g,err}} = \int_0^t (n_g - n_{g,max}) dt, \quad \forall n_g > n_{g,max} \quad (42)$$

The corresponding guidance effort can be represented by the integrated angle of attack and bank angle over time, see Fig. 7(b). Here, the total guidance effort is considered, *i.e.*, the summation of nominal and tracking command, because the nominal guidance command is in principle affected by the tracking and should therefore be taken into account. These indices are thus defined as:

$$\sum_{\alpha} = \int_0^{t_{final}} \alpha_c dt \quad \sum_{\sigma} = \int_0^{t_{final}} \sigma_c dt \quad (43)$$

It is obvious that these metrics should all be as small as possible. Note that since both  $\alpha_c$  and  $\sigma_c$  are always positive (lateral guidance is not considered and  $\alpha_{min} = 10^\circ$ ), there is no need to take the absolute value. Other parameters of interest are the final flight time,  $t_f$ , as possible indicator why  $Q$  is large or not, and the maximum overshoot values of  $q_c$  and  $n_g$ . The extent to which these constraints are overshoot give an indication that thermo-mechanical failure may be expected. A very large overshoot for only a short time may still lead to failure, even if the integrated constraint-violation is small.

For the combination of nominal guidance and LQY tracking, a Monte-Carlo analysis consisting of 500 samples has been executed with the variations in  $\Delta m$ ,  $\Delta \rho$ ,  $\Delta a$ ,  $\Delta C_D$ , and  $\Delta C_L$  mentioned above. The resulting integrated heat-flux deviation and the total heat load are shown in Fig. 8. Most samples for the LQY have values corresponding with the nominal performance<sup>c</sup>. The maximum overshoot of the heat flux is only  $\Delta q_c \approx 80 \text{ kW/m}^2$ . The integrated heat-flux tracking error seems large, but is easily explained and does not pose a danger to the vehicle. Due to the uncertainties in aerodynamics and density, it is not always

<sup>c</sup>For the nominal mission, the performance indices read:  $Q = 1305.3 \text{ MJ/m}^2$ ,  $q_{c,max} = 1703.9 \text{ kW/m}^2$ ,  $\sum_{q_{c,err}} = 3.0 \text{ MJ/m}^2$ ,  $n_{g,max} = 3.67$ ,  $\sum_{n_{g,err}} = 0$ ,  $t_f = 971.7 \text{ s}$ ,  $\sum_{\alpha_c} = 24,185^\circ\text{s}$ , and  $\sum_{\sigma_c} = 54,230^\circ\text{s}$ . Heat-flux tracking is active between  $t_1 = 194.2 \text{ s}$  and  $t_2 = 807.7 \text{ s}$ .

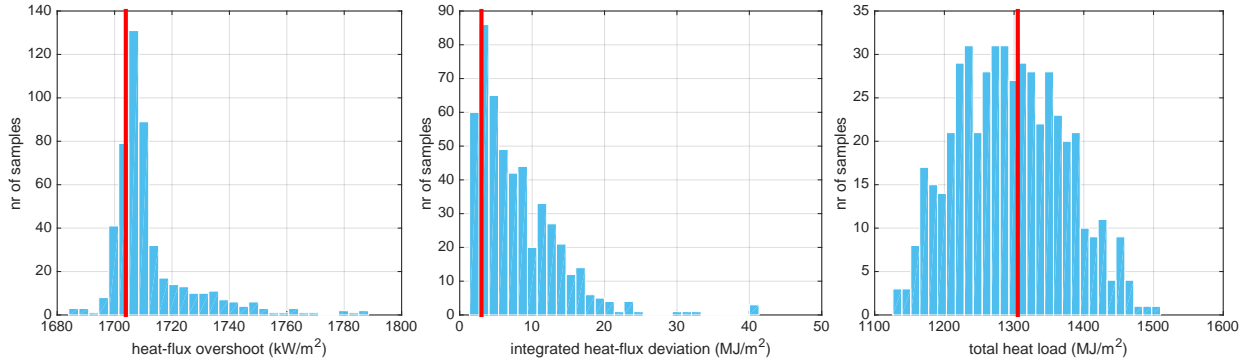


**Figure 8.** *Hyperion-1* sensitivity-analysis results. Red line represents nominal mission.

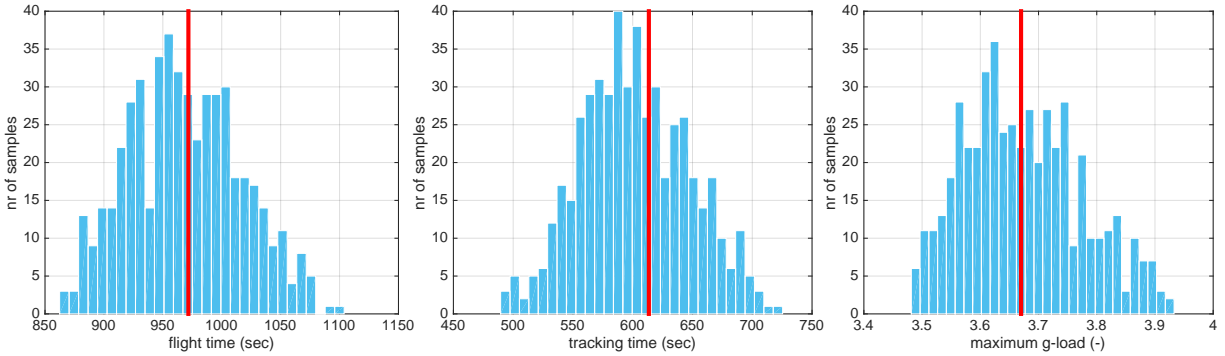


**Figure 9.** *Hyperion-1* sensitivity-analysis results - Concluded. Red line represents nominal mission.

possible to track the set point of  $1,700 \text{ kW/m}^2$ , instead a (mostly) lower constant flux is tracked. Because the integrated error is related to the original set point and the tracking time is relatively long (between 500 and 700 s), this easily leads to large integrated errors. A redesign of the nominal guidance, where a set point can be dynamically determined based on the (maximum) capabilities of the vehicle would solve this, and also alleviate the control load on the tracking system.

The variation for the integrated heat load is restricted to  $\pm 10\%$ , which fits well within the design margins of TPS mass during the conceptual design phase. The variation in  $Q$  is, of course, directly linked with the total flight time and heat-flux tracking time, shown in Fig. 9. A larger flight time will, for a given set point, automatically lead to a larger heat load. The variation in  $t_f$  of about  $\pm 10\%$  corresponds in that sense well with the variation in  $Q$ . Furthermore, also a larger tracking time will, in general, increase the tracking error (with the exception of perfect tracking, of course). Inspecting the combination of the variables does indeed show this dependency, which leads to the conclusion that the overall performance of the guidance system is consistent. The last plot in Fig. 9 shows the maximum  $g$ -load. It is particularly interesting to see that in none of the 500 flights the  $g$ -load exceeds the limit value of  $n_{g,max} = 5$ . The modifications in, most notably, the nominal guidance have proved to be effective.

In terms of guidance effort, in Fig. 10 the integrated angle-of-attack and bank-angle commands are plotted. The variation is around  $\pm 20\%$ . This spread is relatively large, indicating that for some trajectories significant guidance corrections may be required. However, also in this case a longer flight time will automatically substantially increase the guidance effort. For all 500 trajectories no particular outliers were found that might indicate a guidance problem.

The next logical step would be to study whether the original Model Reference Adaptive Guidance (MRAG) system, as well as the integration with the LQY, as discussed in Ref. 5, will be able to reduce the guidance effort, and hopefully at the same time reduce the variation in the other performance criteria as well. An example of the difference in performance between the three tracking systems is shown in Fig. 11, with the integrated heat load as performance indicator (given the same uncertainties in the Monte-Carlo simulations).

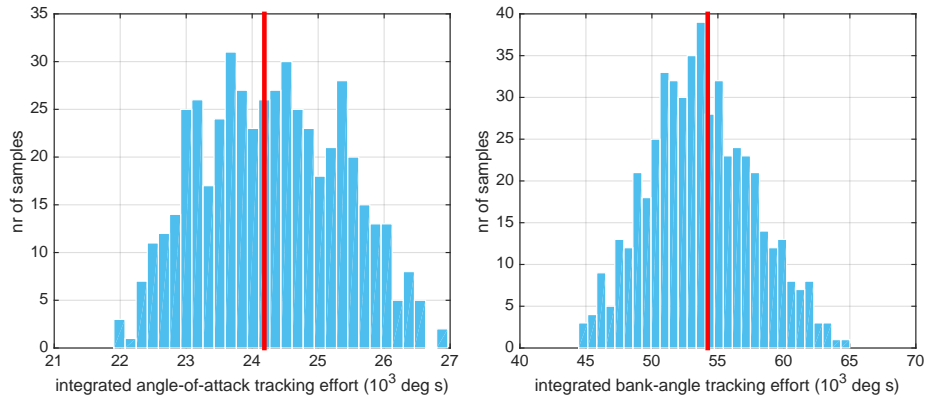


Figure 10. *Hyperion-1* guidance effort. Red line represents nominal mission.

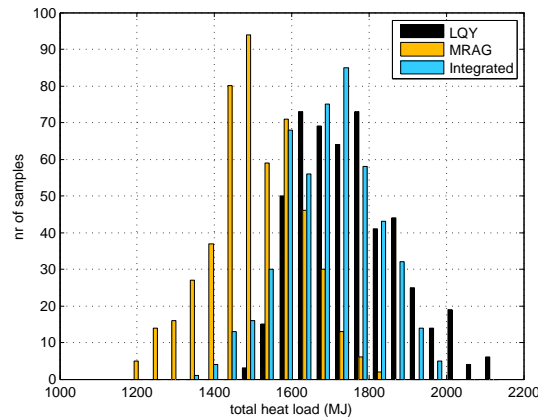


Figure 11. Original *Hyperion-1* integrated heat-load results.<sup>5</sup>

In between the three, the MRAG tracking system performs best, albeit at an increase in guidance effort. The integration with the LQY did not give so much performance benefit compared to the standalone LQY, although it is fair to say that the integrated tracking error was reduced. Also the MRAG design parameters were not fully optimised. Looking at the current LQY results,  $Q$  has reduced substantially compared to the original MRAG results, albeit the guidance effort for the current implementation has increased. However, the original results for the  $g$ -load showed some large overshoots, but as mentioned above, in the current implementation this constraint is never violated.

To study the link between the nominal and the tracking guidance a bit more, we increase the uncertainties. The applied uncertainties that are taken into account are the vehicle mass ( $\pm 20$  kg), the atmospheric density ( $\pm 25\%$ ), the speed of sound ( $\pm 10\%$ ), the drag and lift coefficient ( $\pm 20\%$ ), and in this case also the entry velocity ( $\pm 20$  m/s) and entry flight-path angle ( $\pm 0.1^\circ$ ) all with a uniform distribution. Since it was already established that the induced errors will have an impact on the nominal guidance commands, the goal is now to find out whether the tracking guidance can handle this.

Figure 12 shows the thermal-performance related criteria. Also with these increased uncertainties the guidance system performs well, although all variations have increased. The maximum heat-flux overshoot is around  $200 \text{ kW/m}^2$ , which is caused by the change in entry flight-path angle, and not the "failing" of the guidance system. Given the entry conditions, the heat-flux guidance is only activated after passing the maximum heat-flux peak, and without increasing the angle of attack (or, effectively, the lift) this peak value is a given. To confirm this, in Fig. 13 the resulting heat-flux profiles of all 500 runs have been plotted. Overshoots are indeed limited, although there are quite some excursions to values much lower than the set point. Even though these (low-frequency) oscillations do not cause any guidance problems, a tighter constraint tracking is necessary so a more robust guidance system would be required to keep the TPS mass

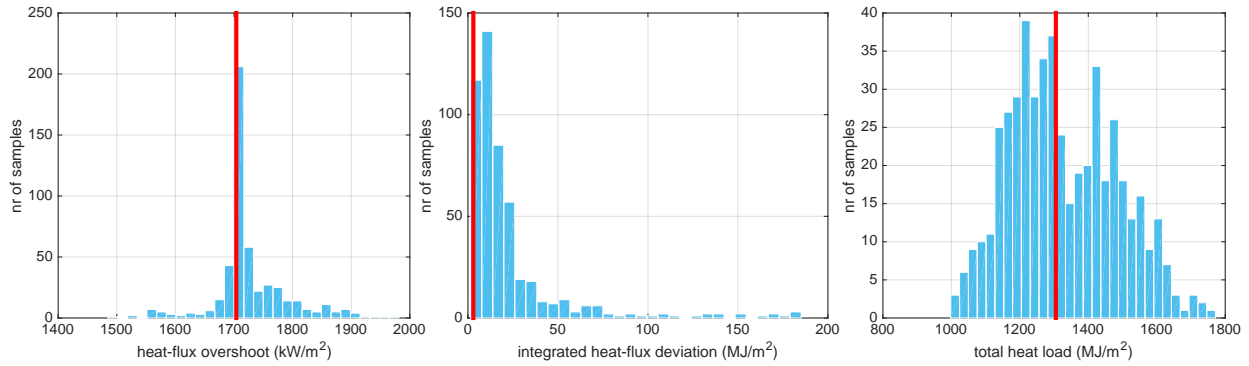


Figure 12. *Hyperion-1* worst-case sensitivity-analysis results. Red line represents nominal mission.

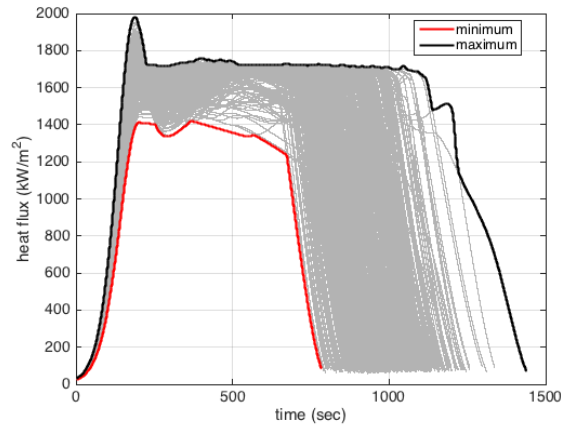


Figure 13. Heat-flux profiles for all 500 worst-case Monte-Carlo simulations, including the encapsulating minimum and maximum curves.

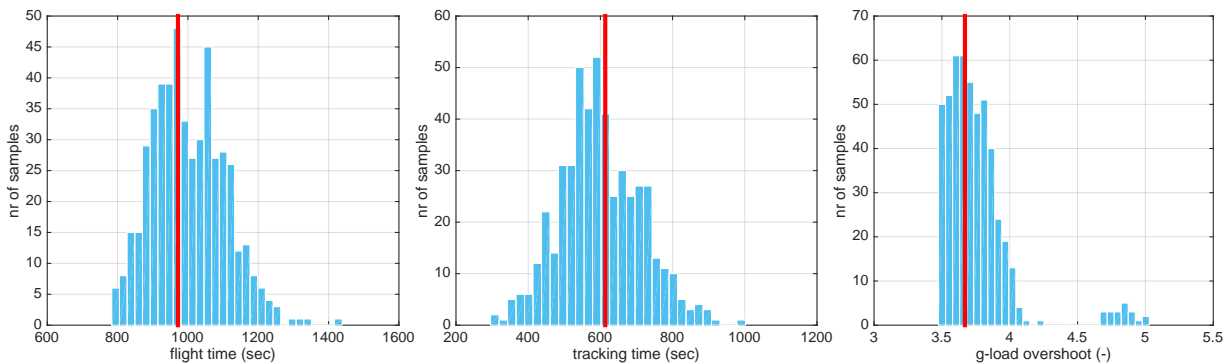


Figure 14. *Hyperion-1* worst-case sensitivity-analysis results - Concluded. Red line represents nominal mission.

within its design margins.

To conclude the discussion, also with these much larger dispersions the maximum *g-load* is never violated (Fig. 14). The guidance effort (Fig. 15) has increased, but compared to Fig. 10 not dramatically so. All in all, it can be safely said that despite not being optimal, the performance of the guidance system is consistent and can handle large dispersions relatively well.

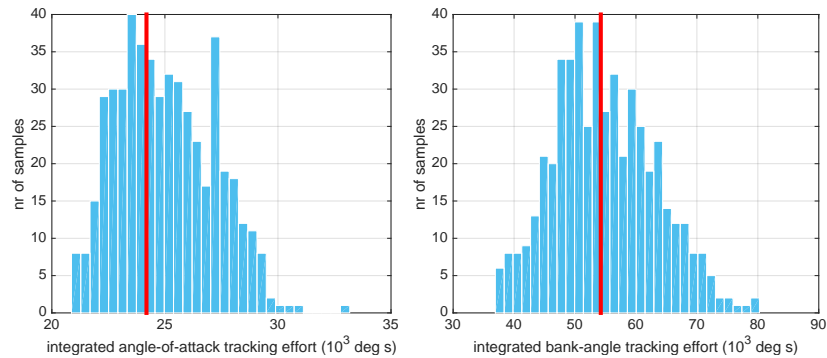


Figure 15. *Hyperion-1* worst-case guidance effort. Red line represents nominal mission.

## V. Conclusions and Recommendations

In this paper the heat-flux tracking for a hypersonic test vehicle called *Hyperion-1*, is studied. Tracking is done by a (linear) output-feedback controller (LQY). Improvements in the nominal guidance as well as the tracking system have improved the performance with respect to earlier results. These improvements deal with the transition from heat-flux tracking to constraining the maximum  $g$ -load using a smooth step function, a PID regulator on the flight-path angle error, and a PD regulator on the heat-flux error. Both the heat-flux and  $g$ -load constraints are well observed, and the integrated heat-load variation is well within the margins during the conceptual design phase.

Future work could focus on the redesign and optimisation of an adaptive tracking system, preferably by setting up an automated design methodology. This adaptive system could then also be used as an outer loop around the LQY to combine the strong points of each individual tracking system. Since the nominal guidance is linked with the vehicle state (and thus the tracking guidance), starting point should be to study how the nominal guidance can be made more robust and decoupled from the tracking guidance. One potential change could be to have a variable constraint value, but as close to the maximum constraint value as possible. This would avoid excessive commands to reach this value if the vehicle performance does no longer allow for it. The current implementation of the guidance algorithm allows for discrete jumps in certain parameters. Smooth step functions or low-pass filters could be used to improve performance robustness.

## References

- <sup>1</sup>Kaufman, H., Barkana, I. and Sobel, K., *Direct adaptive control algorithms: Theory and applications*, Second edition, Springer-Verlag, New York, 1998.
- <sup>2</sup>Barkana, I., "Classical and Simple Adaptive Control for Non-Minimum Phase Autopilot Design", *Journal of Guidance, Control, and Dynamics*, Vol. 24, No. 4, pp. 631-638, July-August 2004.
- <sup>3</sup>Mooij, E., "Simple Adaptive Bank-Reversal Control of a winged Re-entry Vehicle", AIAA-04-4869, *AIAA Guidance, Navigation, and Control Conference*, Providence, RI, August 16-19, 2004.
- <sup>4</sup>Mooij, E., "Robustness Analysis of an Adaptive Re-entry Guidance System", AIAA-05-6146, *AIAA Guidance, Navigation, and Control Conference*, San Francisco, CA, August 15-18, 2005.
- <sup>5</sup>Mooij, E., "Adaptive Heat-Flux Tracking for Re-entry Guidance", AIAA-2014-4142, *AIAA/AAS Astrodynamics Specialist Conference*, San Diego, CA, August 4-7, 2014.
- <sup>6</sup>Mooij, E., Maree, A.G.M. and Sudmeijer, K.J., "Aerodynamic controllability of a selected re-entry test vehicle", IAF-95-V.4.04, *46<sup>th</sup> International Astronautical Congress*, Oslo, Norway, October 2-6, 1995.
- <sup>7</sup>Mooij, E., Kremer, F.J.G. and Sudmeijer, K.J., "Aerodynamic design of a low-cost re-entry test vehicle using a Taguchi approach", AIAA-99-4831, *AIAA 9<sup>th</sup> International Space Planes and Hypersonic Systems and Technologies Conference*, Norfolk, VA, 1999.
- <sup>8</sup>Vinh, N.X., *Optimal trajectories in atmospheric flight*, Elsevier scientific publishing company, 1981.
- <sup>9</sup>Ebert, D.S., Musgrave, F.K., Peachey, D., Perlin, K., and Worley, S., *Texturing & Modeling: A Procedural Approach*, Third Edition, Ch. 12, "Noise, Hypertexture, Antialiasing, and Gesture", Morgan Kaufmann Publishers, 2003.